2020 American Control Conference
Denver, CO, USA, July 1-3, 2020

Optimal Sample-Error/Ripple Tradeoff for Sampled-Data Systems with Harmonic Disturbances

Nima Mohseni and Dennis S. Bernstein

Abstract— **Although a digital controller operating in a sampled-data control system has access to the sampled error signal, the intersample behavior (ripple) is relevant to the overall performance. This paper thus investigates the tradeoff between the sample error and ripple for a system with a lightly damped mode and harmonic disturbance. The approach is based on an approximate expression for the harmonic-steady-state response of the closed-loop system. Numerical optimization of the ripple provides an optimal tradeoff between the peak sample error and peak ripple. Fast sampling as well as the effect of modal folding and disturbance aliasing are considered.**

I. Introduction

For control applications involving continuous-time plants, the control system is typically implemented with a digital controller connected through analog-to-digital (A/D) and digital-to-analog (D/A) devices. The resulting sampled-data control system thus has access to the error signal at the sampling times, but not between samples. The intersample behavior contributes to the performance of the control system in practice, however, and thus its magnitude must be taken into account in the design process [1], [2], [3].

In steady-state operation, the intersample behavior is called *ripple*, and it has been shown that, in special cases, it is possible to reduce the ripple to zero [4], [5], [6], [7]. However, these are special cases focusing on tracking, and thus it is almost always the case that the ripple is nonzero in the case of a harmonic disturbance. This raises the question as to the extent to which it is possible to suppress ripple [8].

One approach to suppressing the intersample magnitude is to synthesize feedback controllers that are optimal in the sense of the induced H_2 and H_∞ norms of the sampled-data system [9], [10], [11]. As stated in [11, p. 160], "optimal design based on discrete performance specs alone may be ill-posed because intersample behaviour is completely ignored and the behaviour at sampling instants is over-emphasized."

The present paper considers a more limited problem, where the disturbance is a single harmonic and the plant consists of a single lightly damped mode. For plants of this type, which may be reminiscent of a vibrating structure subject to harmonic periodic disturbances, it is often the case that either the disturbance frequency or the modal frequency lies above the Nyquist rate. This situation gives rise to either modal folding or disturbance aliasing. The usual approach in practice is to include an anti-aliasing filter to attenuate the effect of modal folding and disturbance aliasing. As stated in [11, p. 30], "it is a good idea to include [an antialiasing filter] at the start of the analog design so that there are no surprises later due to additional phase lag." However, an antialiasing filter cannot completely remove these effects. It should be mentioned that sampling causes folding whether or not a lightly damped mode is present in the system. In particular, the discrete-time frequency response of a linear continuous-time plant discretized with sampling and zero-order-hold signal reconstruction is determined by the folding of all dynamics above the Nyquist frequency.

The present paper focuses on the problem of harmonic disturbance rejection with and without modal folding and disturbance aliasing. The objective of this work is to assess the tradeoff between the error at the sampling times and the intersample error. To do this, we focus on the peak sample error and the peak ripple for the harmonic steady-state response of the system. The tradeoff is assessed by optimizing controllers based on an approximate expression for the hamonic steady-state response of the sampled-data system.

The contents of the paper are as follows. Section II defines the problem formulation in terms of the underlying continuous-time system and its discretization with A/D and D/A devices. Section III analyzes the harmonic-steady-state response of the closed-loop system. Section IV presents numerical optimization of the controller under fast sample, while sections V, VI, and VII consider the cases of modal folding and/or disturbance aliasing. Conclusions are given in Section VIII.

II. Problem Statement

Consider the SISO continuous-time linear time-invariant system

$$\dot{x}(t) = Ax(t) + B(u(t) + w(t)), \tag{1}$$

$$y(t) = Cx(t). \tag{2}$$

where $x(t) \in \mathbb{R}^n$ is the state, $u(t) \in \mathbb{R}$ is the control input, $w(t) \in \mathbb{R}$ is the disturbance, and $y(t) \in \mathbb{R}$ is the measurement. Note that the disturbance and control input are matched, and that the measurement is noise-free. Let G denote the continuous-time transfer function from $u + w$ to y.

The system (1), (2) is controlled by a discrete-time feedback controller in a sampled-data feedback loop. The measurement y is sampled at the sampling times $0, T_\mathrm{s}, 2T_\mathrm{s}, \ldots,$ and the control input is provided by zero-order-hold signal

The authors are with the Department of Aerospace Engineering, University of Michigan, Ann Arbor, MI 48109.

reconstruction. The discretized dynamics thus have the form

$$x_{\rm d}(k+1) = A_{\rm d}x_{\rm d}(k) + B_{\rm d}(u_{\rm d}(k) + w_{\rm d}(k)), \tag{3}$$
$$y_{\rm d}(k) = Cx_{\rm d}(k), \tag{4}$$

where $x_{\rm d}(k) \triangleq x(kT_{\rm s})$, $y(k) \triangleq y(kT_{\rm s})$, and $u_{\rm d}$ is the discrete-time control input. The matrices $A_{\rm d}$ and $B_{\rm d}$ of the discrete-time dynamics are given by

$$A_{\rm d} \triangleq e^{AT_{\rm s}}, \quad B_{\rm d} \triangleq \int_0^{T_{\rm s}} e^{At}{\rm d}tB. \tag{5}$$

If A is nonsingular, then

$$B_{\rm d} \triangleq A^{-1}(A_{\rm d} - I)B. \tag{6}$$

Let $G_{\rm d}$ denote the discrete-time transfer function from $u_{\rm d}$ to $y_{\rm d}$. Furthermore, the discrete-time disturbance signal is given by [12]

$$w_{\rm d}(k) \triangleq \int_{(k-1)T_{\rm s}}^{kT_{\rm s}} e^{A(kT_{\rm s}-t)}Bw(t)\,{\rm d}t. \tag{7}$$

For this paper, the dynamics consist of a single lightly damped mode modeled by

$$A = \begin{bmatrix} 0 & 1 \\ -\omega_{\rm n}^2 & -2\zeta\omega_{\rm n} \end{bmatrix}, \; B = \begin{bmatrix} 0 \\ 1 \end{bmatrix}, \; C \; = [1 \;\; 0], \tag{8}$$

where $\omega_{\rm n}$ is the natural frequency and ζ is the damping ratio. The disturbance w is the harmonic signal

$$w(t) = \alpha\sin(\omega_{\rm d}t + \phi) \tag{9}$$

with amplitude α, frequency $\omega_{\rm d}$, and phase shift ϕ. The feedback controller is a linear SISO discrete-time controller $G_{\rm c}$. The discrete-time closed-loop transfer function $\tilde{G}_{y_{\rm d},w_{\rm d}}$ from $w_{\rm d}$ to $y_{\rm d}$ is thus given by

$$\tilde{G}_{y_{\rm d}w_{\rm d}} = \frac{G_{\rm d}}{1 + G_{\rm d}G_{\rm c}}. \tag{10}$$

III. Analysis of the Closed-Loop Harmonic-Steady-State Response

The closed-loop sampled-data system is shown in Figure 1a, where

$$G_{\rm zoh}(s) = \frac{1 - e^{-sT_{\rm s}}}{s} \tag{11}$$

is the transfer function for the zero-order-hold. The combined transfer function of the continuous-time dynamics and zero-order hold is given by

$$G_{\rm h}(s) \triangleq G(s)G_{\rm zoh}(s). \tag{12}$$

Using (11), the output of the closed-loop system in Figure 1 is given by

$$\hat{y}(s) = G(s)\hat{w}(s) + G_{\rm h}(s)\hat{u}_{\rm d}(e^{sT_{\rm s}}), \tag{13}$$

where

$$\hat{u}_{\rm d}(z) = -G_{\rm c}(z)\hat{y}_{\rm d}(z). \tag{14}$$

The Z-transform of the sampled impulse response of (13) is given by

$$\hat{y}_{\rm d}(z) = [G\hat{w}](z) + G_{\rm d}(z)\hat{u}_{\rm d}(z), \tag{15}$$

where $[G\hat{w}](z)$ is the Z-transform of the sampled impulse response of $G(s)\hat{w}(s)$ [13, pp. 385–390].

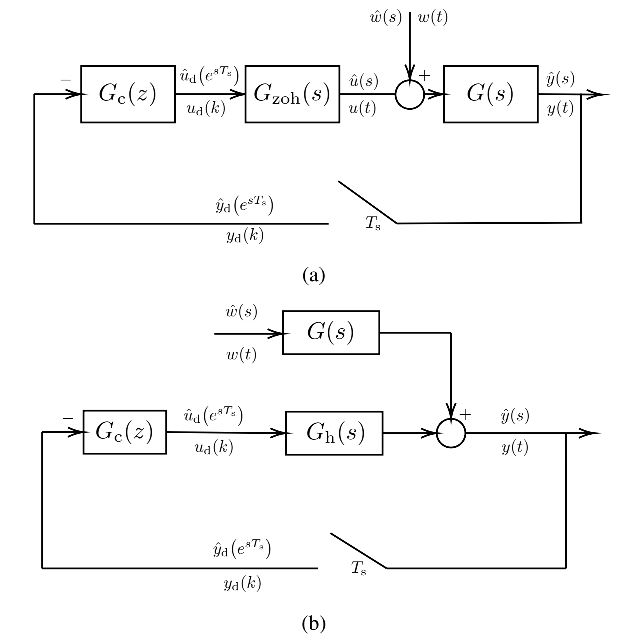

Fig. 1. (a) shows the block diagram of the closed-loop sampled-data system. (b) shows an equivalent block diagram, where the continuous-time dynamics are merged with the zero-order hold.

Next, using (15) and the fact that

$$\hat{u}_{\rm d}(z) = -G_{\rm c}(z)\hat{y}_{\rm d}(z), \tag{16}$$

$\hat{u}_{\rm d}(z)$ can be written as

$$\hat{u}_{\rm d}(z) = -G_{\rm c}(z)[G\hat{w}](z) - G_{\rm c}(z)G_{\rm d}(z)\hat{u}_{\rm d}(z), \tag{17}$$

which yields

$$\hat{u}_{\rm d}(z) = -G_{u_{\rm d}}(z)[G\hat{w}](z), \tag{18}$$

where

$$G_{u_{\rm d}}(z) \triangleq \frac{G_{\rm c}(z)}{1 + G_{\rm c}(z)G_{\rm d}(z)}. \tag{19}$$

Now, substituting $\hat{u}_{\rm d}(e^{sT_{\rm s}})$ into (13) yields

$$\hat{y}(s) = G(s)\hat{w}(s) - G_h(s)G_{u_{\rm d}}(e^{sT_{\rm s}})[G\hat{w}](e^{sT_{\rm s}}). \tag{20}$$

Note that, since $\hat{w}(s)$ cannot be factored out of (20), there does not exist a transfer function from $\hat{w}(s)$ to $\hat{y}(s)$. The second term on the right hand side of (20) is represented by the block diagram shown in Figure 2.

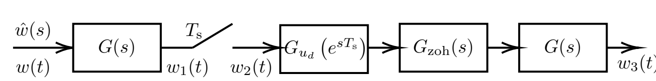

Fig. 2. Block diagram representing the second term on the right hand side of (20).

The output of Figure 2 with the input given by the harmonic disturbance (9) can be constructed as follows. First, let w_1 denote the output of $G(s)$ due to w. Next, the harmonic-steady-state response of G due to w undergoes a magnitude and phase shift, which yields the harmonic response

$$w_{\rm 1ss}(t) \triangleq \alpha|G(\jmath\omega_{\rm d})|\sin(\omega_{\rm d}t + \phi + \angle G(\jmath\omega_{\rm d})). \tag{21}$$

The signal w_1 passes through the sampler, yielding the weighted impulse train

$$w_2(t) \triangleq w_1(t) \sum_{i=-\infty}^{\infty} \delta(t - iT_{\rm s}). \tag{22}$$

The harmonic-steady-state response $w_{2\rm ss}$ of the sampler is given by

$$w_{2\rm ss}(t) \triangleq w_{1\rm ss}(t) \sum_{i=-\infty}^{\infty} \delta(t - iT_{\rm s}), \tag{23}$$

which has the Fourier series

$$w_{2\rm ss}(t) \triangleq \alpha |G(\jmath\omega_{\rm d})| \frac{1}{T_{\rm s}} \sum_{i=-\infty}^{\infty} \sin(\omega_i t + \phi + \phi_i + \angle G(\jmath\omega_{\rm d})), \tag{24}$$

where, for all $-\infty < i < \infty$,

$$\omega_i \triangleq |\omega_{\rm d} - i\omega_{\rm s}|\,, \tag{25}$$

where $\omega_{\rm s} \triangleq \frac{2\pi}{T_{\rm s}}$ and ϕ_i is the associated phase shift caused by the sampler at the frequency ω_i. The cascade of $G_{u_{\rm d}}(e^{sT_{\rm s}})$, $G_{\rm zoh}$, and $G(s)$ affects every frequency ω_i, with a magnitude and phase shift associated with the respective frequency [14]. In particular, the harmonic-steady-state impulse response of the second term on the right hand side of (20) is given by

$$\begin{aligned} w_{3ss}(t) \triangleq \alpha |G(\jmath\omega_{\rm d})| \frac{1}{T_{\rm s}} \sum_{i=-\infty}^{\infty} \big[&|G(\jmath\omega_i)||G_{\rm zoh}(\jmath\omega_i)| \\ &\cdot |G_{u_{\rm d}}(e^{\jmath\omega_i T_{\rm s}})| \sin(\omega_i t + \phi + \phi_i + \angle G(\jmath\omega_{\rm d}) \\ &+ \angle G_{u_{\rm d}}(e^{\jmath\omega_i T_{\rm s}}) + \angle G_{\rm zoh}(\jmath\omega_i) + \angle G(\jmath\omega_i)) \big]. \end{aligned} \tag{26}$$

Using (26), the harmonic-steady-state closed-loop response of the sampled-data system is given by

$$\begin{aligned} y_{\rm hss}(t) \triangleq \alpha |G(\jmath\omega_{\rm d})| \Bigg[&\sin(\omega_{\rm d} t + \phi + \angle G(\jmath\omega_{\rm d})) \\ -\frac{1}{T_{\rm s}} \sum_{i=-\infty}^{\infty} &\big[|G(\jmath\omega_i)||G_{\rm zoh}(\jmath\omega_i)||G_{u_{\rm d}}(e^{\jmath\omega_i T_{\rm s}})| \sin(\omega_i t + \phi + \phi_i \\ &+ \angle G(\jmath\omega_{\rm d}) + \angle G_{u_{\rm d}}(e^{\jmath\omega_i T_{\rm s}}) + \angle G_{\rm zoh}(\jmath\omega_i) + \angle G(\jmath\omega_i)) \big] \Bigg]. \end{aligned} \tag{27}$$

A truncated version of this expression will be used in the next section to minimize the ripple.

IV. Sample-Error/Ripple Tradeoff under Fast Sampling

We consider the continuous-time plant (8) with natural frequency $\omega_{\rm n} = 2\pi$ rad/s, damping ratio $\zeta = 0.05$, and disturbance frequency $\omega_{\rm d} = 2\pi$ rad/s. Furthermore, the sample time is chosen to be $T_{\rm s} = 0.25$ s, and thus $\omega_{\rm s} = 8\pi$ rad/s. Note that the modal frequency $\omega_{\rm n}$ and the disturbance frequency are both below the Nyquist rate $\omega_{\rm Nyq} \triangleq \frac{1}{2}\omega_{\rm s} = \frac{\pi}{T_{\rm s}} = 4\pi$ rad/s.

For disturbance rejection, we use the closed-loop structure shown in Figure 1b by optimizing the coefficients of a discrete-time, second-order controller of the form

$$G_{\rm c}(z) = \frac{az + b}{z^2 + cz + d}. \tag{28}$$

Using (27), the controller that minimizes the peak ripple of the harmonic-steady-state closed-loop response is obtained by solving the optimization problem

$$\begin{aligned} &\underset{a,b,c,d}{\text{minimize}} && J = \max(|y_{\rm hss}(t)|) \\ &\text{subject to} && \rho(\tilde{G}_{y_{\rm d}w_{\rm d}}) < 1, \end{aligned} \tag{29}$$

where ρ denotes the spectral radius. The optimization problem (29) is solved by using the Matlab functions fmincon and GlobalSearch with $y_{\rm hss}(t)$ given by (27) with the summation truncated, where the 1000 lowest frequencies ω_i are retained.

Applying the optimization procedure yields a controller with $J = 0.001134$, more than two orders of magnitude smaller than the open-loop value of 0.2533. The closed-loop frequency response in Figure 4 shows that the controller provides approximately 110 dB of disturbance rejection at the sampling times. The controller is shown in Figure 5 and is similar to an internal model controller. Since the optimization does not enforce closed-loop stability, the resulting controllers can produce an unstable closed-loop response. Controllers that fail to stabilize the loop are shown in red in Figure 3a, and Figure 3b shows only the controllers that stabilize the loop. By retaining stabilizing controllers that are Pareto optimal with respect to peak sample error and peak ripple, the Pareto frontier in Figure 6 shows a tradeoff between the steady-state error at the sampling times and the steady-state error of the ripple.

V. Sample-Error/Ripple Tradeoff under Disturbance Aliasing

We now consider (1), (2) but now with $\omega_{\rm d} = 10\pi$ rad/s, which aliases to $\omega_{\rm d} = 2\pi$ rad/s. Optimizing the second-order controller (28) under this disturbance yields $J = 0.001055$, which is equal to the open-loop value. With the DC gain of the optimized controller being -5.9790e-06, the optimization reveals that using a second-order controller to suppress peak ripple of the harmonic-steady-state response due to an aliased disturbance does not provide any performance improvement and is evidenced in Figure 8 by the frequency responses of the open-loop and closed-loop systems being nearly identical. The poles and zeros of the optimized controller are shown in Figure 9. All of the controllers that stabilize the closed-loop system are shown in Figure 7, and the corresponding Pareto frontier in Figure 10 shows a tradeoff between the peak harmonic-steady-state error at the sampling times and the peak ripple.

VI. Sample-Error/Ripple Tradeoff under Modal Folding

We now consider (1), (2) but now with $\omega_{\rm n} = 20\pi$ rad/s and $\omega_{\rm d} = 2\pi$ rad/s. The lightly damped mode folds onto the lower frequency dynamics when sampled at $T_{\rm s} = 0.25$ s. Optimizing the second-order controller (28) yields $J = 0.0002186$, a slight reduction from the open-loop cost

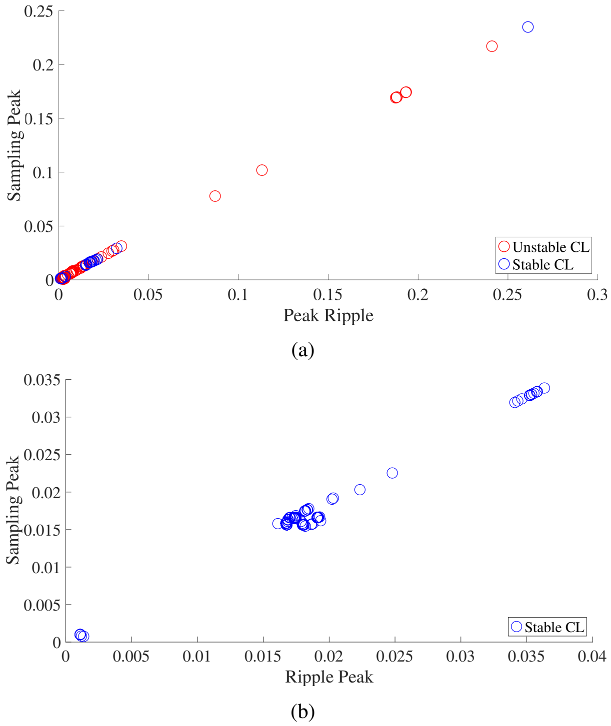

Fig. 3. (a) shows the peak of the harmonic-steady-state response at the sampling times versus the peak of the ripple during each iteration of the global optimization process for the plant (1), (2) under fast sampling. The result of the optimization is the point that minimizes the peak ripple. (b) shows only the points corresponding to asymptotically stable closed-loop systems.

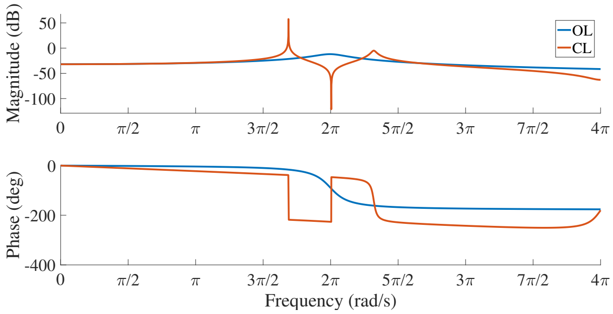

Fig. 4. Bode plots of the open and closed-loop discrete-time systems for the fast sampled plant. Note the anti-resonance of the closed-loop system at the disturbance frequency 2π rad/s.

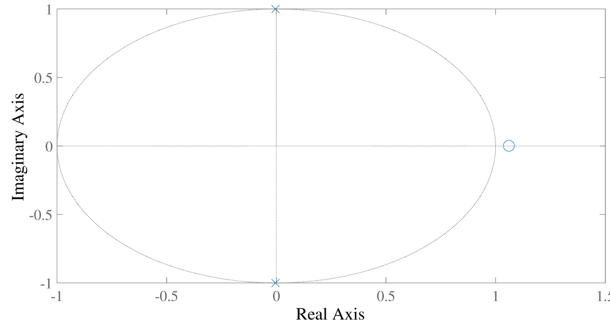

Fig. 5. Pole-zero plot of the optimized controller minimizing the peak ripple for the fast sampled plant. Note that the controller is nearly an internal model controller.

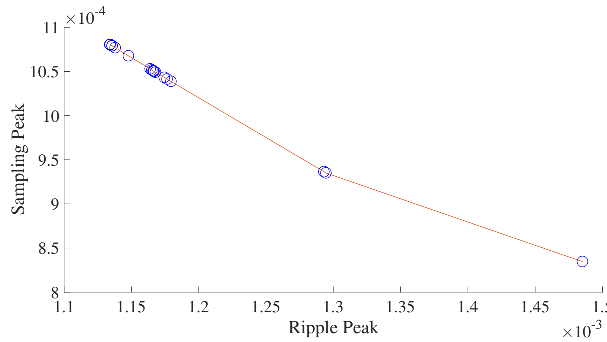

Fig. 6. The Pareto frontier corresponding to the stabilizing controllers for the plant (1), (2) under modal folding for the fast sampled plant. The frontier shows a tradeoff between the peak steady-state error at the sampling times and the peak intersample steady-state error.

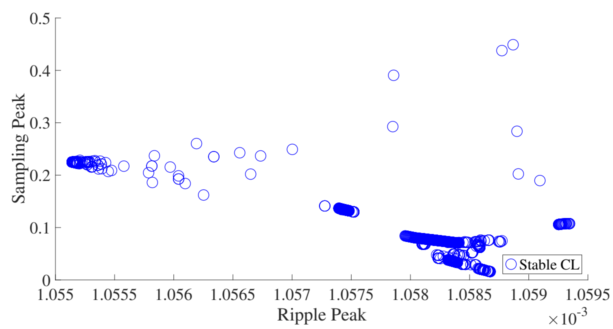

Fig. 7. Stabilizing second-order controllers obtained from the optimization technique for the plant (1), (2) under disturbance aliasing.

$J = 0.0002558$. The frequency response in Figure 12 shows a reduction in amplitude at the disturbance frequency. The pole-zero plot of the optimized controller is shown in Figure 13. All the controllers that stabilize the closed-loop system are shown in Figure 11, and the corresponding Pareto frontier in Figure 14 shows a tradeoff between the peak harmonic-steady-state error at the sampling times and the peak ripple.

VII. Sample-Error/Ripple Tradeoff under Modal Folding and Disturbance Aliasing

Now considering the second-order system with natural frequency $\omega_{\rm n} = 20\pi$ rad/s and disturbance frequency $\omega_{\rm d} = 10\pi$ rad/s. The main plant mode folds onto the lower frequency dynamics, and the disturbance frequency aliases to $\omega_{\rm d} = 2\pi$ rad/s when sampled at $T_{\rm s} = 0.25$ s. Optimizing the second-order controller yields in $J = 0.0003370$, which is equivalent to the magnitude in open-loop harmonic-steady-state. The controller has a DC gain of -1.3602e-05, which again shows that the second-order controller does not provide any performance improvement. This is evidenced by the frequency responses of the open-loop and closed-loop systems being identical as shown in Figure 16. The pole-zero plot of the optimized controller is shown in Figure 17. All of the controllers that stabilize the closed-loop system are shown in Figure 15, and the corresponding Pareto frontier in Figure 18 shows a small tradeoff between peak harmonic-steady-state

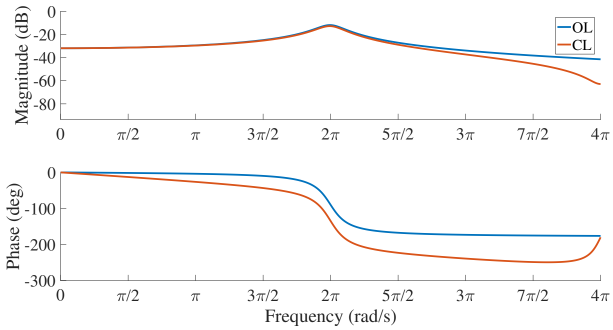

Fig. 8. Bode plots of the open and closed-loop discrete-time systems for the plant (1), (2) under disturbance aliasing. The open and closed-loop frequency responses are nearly equal. Note the controller does not try to perform disturbance rejection of the 10π rad/s disturbance at its associated aliased frequency 2π rad/s.

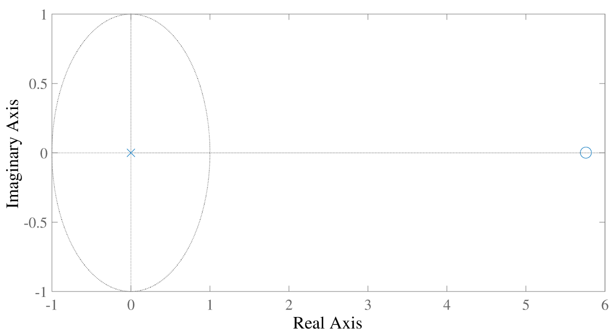

Fig. 9. Pole-zero plot of the optimized controller minimizing the peak ripple for the plant (1), (2) under disturbance aliasing showing that all controller poles were placed near the origin.

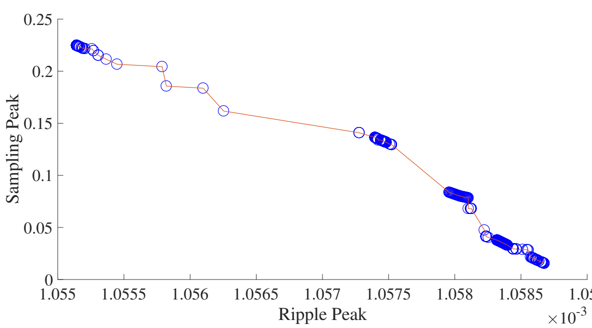

Fig. 10. The Pareto frontier corresponding to the stabilizing closed-loop controllers for the plant (1), (2) under disturbance aliasing. These controllers show a tradeoff between the peak harmonic-steady-state error at the sampling times and the peak ripple.

error at the sampling times and the peak ripple.

VIII. Conclusions and Future Research

This paper investigated the tradeoff between the peak sample error and the peak ripple in the closed-loop harmonic-steady-state response. Four cases were considered, namely, fast sampling, disturbance aliasing, modal folding, and combined modal folding and disturbance aliasing. For each case, parameter optimization was used to obtain controllers whose peak sample error and peak ripple form a Pareto front characterizing the optimal tradeoff between these performance metrics. Table I summarizes the properties of the achievable tradeoff in each case. Future research will explore

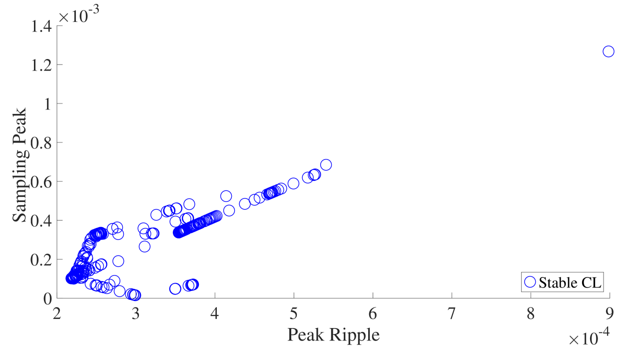

Fig. 11. Stabilizing second-order controllers obtained from the optimization technique for the plant (1), (2) under modal folding.

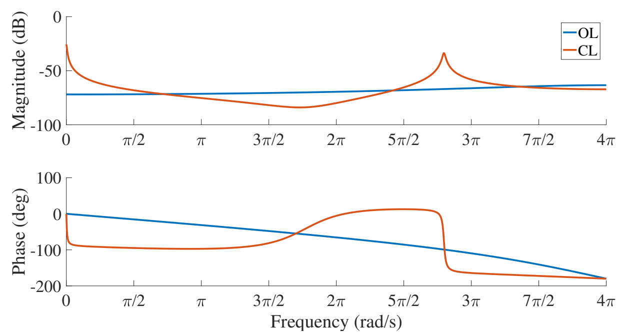

Fig. 12. Bode plots of the open and closed-loop discrete-time systems for the plant (1), (2) under modal folding. Note the slight reduction in magnitude at the disturbance frequency.

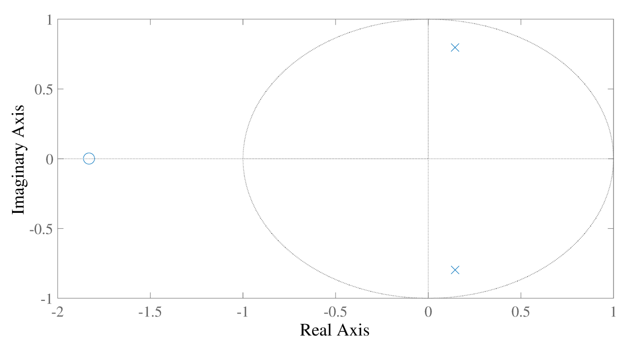

Fig. 13. Pole-zero plot of the optimized controller for the plant (1), (2) under modal folding.

TABLE I

Summary of the Optimization Results

$\omega_{\rm n}$ / $\omega_{\rm d}$	Not Folded	Folded
Not Aliased	Able to minimize peak ripple. Tradeoff between peak sample error and peak ripple exists.	Able to minimize peak ripple by a small amount. Tradeoff between peak sample error and peak ripple exists.
Aliased	Not able to minimize peak ripple. Pareto frontier shows that minimization of peak sample error is possible.	Not able to minimize peak ripple. The Pareto frontier shows small tradeoff between peak sample error and peak ripple.

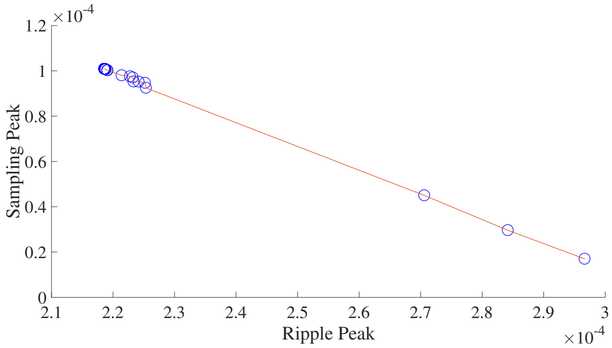

Fig. 14. The Pareto frontier corresponding to the stabilizing controllers for the plant (1), (2) under modal folding. The frontier shows a tradeoff between the peak steady-state error at the sampling times and the peak intersample steady-state error.

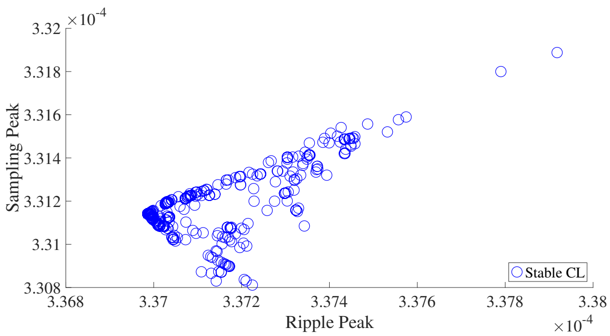

Fig. 15. Stabilizing second-order controllers obtained from the optimization technique for the plant (1), (2) under modal folding and disturbance aliasing.

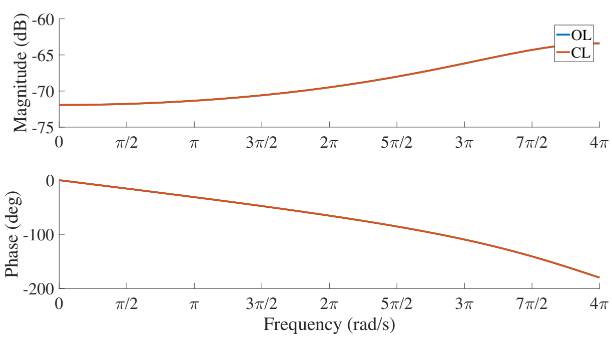

Fig. 16. Bode plots of the open and closed-loop discrete-time systems for the plant (1), (2) with modal folding and disturbance aliasing. Note that the open and closed-loop responses are equal.

the implications of these tradeoffs within the context of adaptive control. A preliminary investigation in this direction is given in [15].

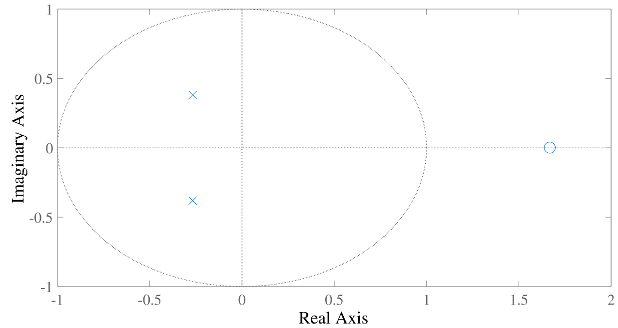

Fig. 17. Pole-zero plot of the optimized controller minimizing the peak ripple for the plant (1), (2) under modal folding and disturbance aliasing.

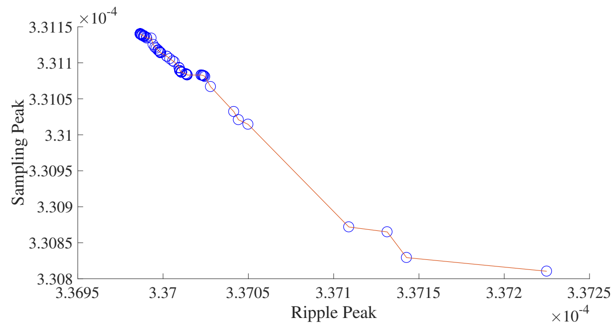

Fig. 18. The Pareto frontier corresponding to the stabilizing controllers for the plant (1), (2) under modal folding and disturbance aliasing. The frontier shows a small tradeoff between the peak steady-state error at the sampling times and the peak intersample steady-state error.

References

[1] T. Sato and S. Masuda, "Generalized predictive control for improving intersample performance," *IEEJ Transactions on Electrical and Electronic Engineering*, vol. 2, no. 6, pp. 620–626, 2007.

[2] K. J. Åström and B. Wittenmark, *Computer-controlled Systems: Theory and Design (2nd Ed.)*. Upper Saddle River, NJ, USA: Prentice-Hall, Inc., 1990.

[3] P. T. Kabamba and S. Hara, "Worst-case analysis and design of sampled-data control systems," *IEEE Trans. Autom. Contr.*, vol. 38, no. 9, pp. 1337–1358, Sep. 1993.

[4] S. Urikura and A. Nagata, "Ripple-free deadbeat control for sampled-data systems," *IEEE Trans. Autom. Contr.*, vol. 32, no. 6, pp. 474–482, June 1987.

[5] A. Casavola, "Robust ripple-free deadbeat control design," *Int. J. Contr.*, vol. 72, no. 6, pp. 564–573, 1999.

[6] M. Salgado, D. Oyarzún, and E. Silva, "H2 optimal ripple-free deadbeat controller design," *Automatica*, vol. 43, pp. 1961–1967, 11 2007.

[7] R. A. Paz, "Ripple-free tracking with robustness," *International Journal of Control*, vol. 79, no. 6, pp. 543–568, 2006.

[8] S. Hara, M. Tetsuka, and R. Kondo, "Ripple attenuation in digital repetitive control systems," in *IEEE Conf. Dec. Contr.*, Dec 1990, pp. 1679–1684 vol.3.

[9] J. Yuz and G. C. Goodwin, *Sampled-Data Models for Linear and Nonlinear Systems*. Springer, 2014.

[10] G. C. Goodwin, J. C. Aguero, M. E. Cea Garridos, M. E. Salgado, and J. I. Yuz, "Sampling and sampled-data models: The interface between the continuous world and digital algorithms," *IEEE Control Systems Magazine*, vol. 33, no. 5, pp. 34–53, Oct 2013.

[11] T. Chen and B. A. Francis, *Optimal Sampled-Data Control Systems*. Springer, 1995.

[12] R. H. Middleton and G. C. Goodwin, *Digital Control and Estimation: A Unified Approach*. Prentice Hall PTR, 1990.

[13] G. C. Goodwin, S. F. Graebe, and M. E. Salgado, *Control System Design*. Prentice Hall, 2000.

[14] E. A. Lee and P. Varaiya, *Structure and Interpretation of Signals and Systems*, 2nd ed. Prentice Hall PTR, 2011, pp. 488–493.

[15] E. D. Sumer and D. S. Bernstein, "Aliasing Effects in Direct Digital Adaptive Control of Plants with High-Frequency Dynamics and Disturbances," in *Proc. Amer. Contr. Conf.*, Washington, DC, June 2013, pp. 4934–4939.